View Article Online
DOI: 10.1039/C3NR03001F

Enhanced and directional emission of semiconductor nanowires tailored through leaky/guided modes

R. Paniagua-Dom´nguez,*[a] G. Grzela,[b‡] J. Gómez Rivas,[b‡] and J. A. Sánchez-Gil[a]

Received Xth XXXXXXXXXX 20XX, Accepted Xth XXXXXXXXX 20XX
First published on the web Xth XXXXXXXXXX 200X
DOI: 10.1039/b000000x

Photoluminescence from finite semiconductor nanowires is theoretically investigated, exploring and predicting their antenna-like properties for light emission in a variety of configurations of interest in Nanophotonics. The theoretical analysis is based on the leaky/guided mode dispersion relation for infinite nanowires, which govern the local density of available electromagnetic states. Light emission from finite nanowires is then numerically investigated in various scenarios with regard to its enhancement and directionality. A simple analytical model is derived that, upon tuning leaky/guided mode coupling through dipole position/orientation and nanowire length, allows us to predict their antenna-like behavior and thus to tailor photoluminescence (including magnetic dipole transitions) at will, with regard to both enhancement/inhibition and associated radiation patterns.

1 Introduction

Semiconductor nanowires (NWs) are attracting an increasing interest in recent years. Among other fascinating applications, this stems from their unique optical properties, which make them specially suitable to selectively enhance light scattering, absorption, and emission at the nanoscale[1,2]. The resulting realm of phenomenology, some in turn in connection with ad-hoc electronic and/or quantum properties, holds promise for potential applications in nanophotonics: single-photon sources[3–6] nanolasers,[7–9] solar light absorbers and photodetectors in photovoltaics,[10–16] antireflection coatings,[17] metamaterials,[18] etc.

Specially relevant to a wealth of applications is the process of photoluminescence mediated by the semiconductor NW geometry[1,8,10,13,19–23]. Typically, light emission is theoretically addressed in the context of light-coupling into guided modes, well known in Electrodynamics for infinitely long NWs[24–26], extended to finite nanowires by taking into account the diffraction resulting from the end-facets of the nanowires[4,8,27–30], which results in a nanowire antenna effect[30]. Very recently, it has been experimentally shown through Fourier microscopy that semiconducting NWs indeed play the role of nanoantennas[22,30], much as their metallic counterparts[31–33], with the obvious advantage of the variety of light emitters allowed to be embedded in semiconductor NWs and low ohmic losses of semiconductors. Such NW antenna emission has been attributed theoretically to coupling into the lowest-order leaky mode supported by the InP NW. However, the emission of finite semiconductor NWs has been neither analytically described nor systematically investigated.

In this work, we explore the vast phenomenology associated to light coupling into the wealth of both leaky and guided modes supported by a finite semiconducting NW. We first discuss theoretically infinitely long nanowires in light of the leaky/guided mode dispersion relation. On this basis, the light emission from finite nanowires is numerically studied for specific configurations, putting special emphasis on the conditions that yield larger enhancement factors and desired directionality. The phenomenology exhibited by light emission mediated by guided mode excitation is much richer, with enhancement factors strongly oscillating as a function of both dipole position and nanowire length. Moreover, we find that the directionality of the emission pattern exhibits lobes governed also by dipole position and nanowire length. We also introduce simple expressions to qualitatively and quantitatively describe the resulting rich phenomenology, thus yielding simple means to tune photoluminescence enhancement and directionality. Similar expressions have been used to describe outside fluorescence emitters coupled to the transverse-magnetic plasmon mode of a metallic nanoantenna[34]. However, the formalism we introduce is general and accounts for all dipole orientations and related mode symmetries in any finite, metallic or dielectric nanowire. Interestingly, magnetic dipole emission, as is the case of spontaneous emission from lantanides[35], is also addressed. Light emission mediated by leaky mode excitation, on the other hand, is shown to weakly depend on the dipole position and nanowire length (except at distances from the NW edge smaller than the mode propa-

[a] *Instituto de Estructura de la Materia, Consejo Superior de Investigaciones Cientficas, IEM-CSIC, Serrano 121, 28006 Madrid, Spain. Fax: 34 915645557; Tel: 34 915616800; E-mail: ramon.paniagua@iem.cfmac.csic.es, j.sanchez@csic.es*
[b] *FOM Institute for Atomic and Molecular Physics (AMOLF), c/o Philips Research Labs, High-Tech Campus 4, 5656 AE Eindhoven, The Netherlands.*

View Article Online
DOI: 10.1039/C3NR03001F

gation length). Altogether, unlike previous work, we give a unified picture on finite-nanowire photoluminescence encompassing coupling into both leaky and guided modes through simple quasi-analytical expressions. These expressions will allow experimentalists to predict the total (angular and spectral) radiated power and Purcell factors as a function of emission position/orientation and nanowire length.

2 In nite cylinders: Leaky/guided modes

First of all, we study the optical properties of infinitely long semiconducting nanowires through the supported leaky/guided modes. Electromagnetic modes in cylinders of radius R are obtained by solving the dispersion relation[24]:

$$\left[\frac{\mu_c}{k_cR}\frac{J_m(k_cR)}{J_m(k_cR)}-\frac{\mu}{kR}\frac{H_m(kR)}{H_m(kR)}\right]\times\left[\frac{\epsilon_c}{k_cR}\frac{J_m(k_cR)}{J_m(k_cR)}-\frac{\epsilon}{kR}\frac{H_m(kR)}{H_m(kR)}\right]=m^2\frac{(k_zR)^2}{(\omega R/c)^2}\left[\frac{1}{(kR)^2}-\frac{1}{(k_cR)^2}\right]^2 \quad (1)$$

where m is an integer, and J_m and H_m standard Bessel and (first-kind) Hankel functions; $k_c=[\epsilon_c(\omega/c)^2-k_z^2]^{1/2}$ and $k=[\epsilon(\omega/c)^2-k_z^2]^{1/2}$ are the transverse components of the mode wavevectors inside (k_c) and outside (k) the cylinder, respectively, $k_z=k_z+\imath k_z$ being the mode complex wavevector along the cylinder axis and $\omega/c=2\pi/\lambda$ (λ is the wavelength in vacuum). The dielectric permittivities and magnetic permeabilities of the cylinder and embedding medium are ϵ_c,μ_c and ϵ,μ, respectively, with corresponding refractive indices $n_c=(\epsilon_c\mu_c)^{1/2}$ and $n=(\epsilon\mu)^{1/2}$. Throughout the rest of the paper, we assume the embedding medium to be vacuum $n=1$ and nonmagnetic cylinders ($\mu_c=\mu=1$). Thus modes with $k_z<\omega/c$ ($k_z>\omega/c$) are leaky (guided), assuming that $k_z\ll k_z$.

Let us focus on an InP nanowire in vacuum at $\lambda=880$ nm. The InP refractive index[36] is assumed to be $n_c=n_{\rm InP}=3.42$. The dispersion relation is calculated from Eq. 1. This means that, strictly speaking, the nanowire radius R is the independent variable, whereas $\omega/c=2\pi/\lambda$ remains fixed; alternatively, as long as the refractive index remains constant, the resulting dispersion relation can be also applied to a proper spectral dependence for fixed nanowire radius.

The results are shown in Fig. 1: the light line $\omega/c=k_z$ (black dashed line in the figure) separates the guided modes (outside the light cone) from the leaky modes $k_z<\omega/c$ (inside the light cone). Guided modes are characterized by parallel wavevectors $k_z\geq\omega/c$ [with $k_z=0$ for absorptionless NWs, $(\epsilon_c)=0$] so that their wavevector in the embedding medium is purely imaginary ($k=0$), precluding coupling into propagating waves outside the NW. By contrast,

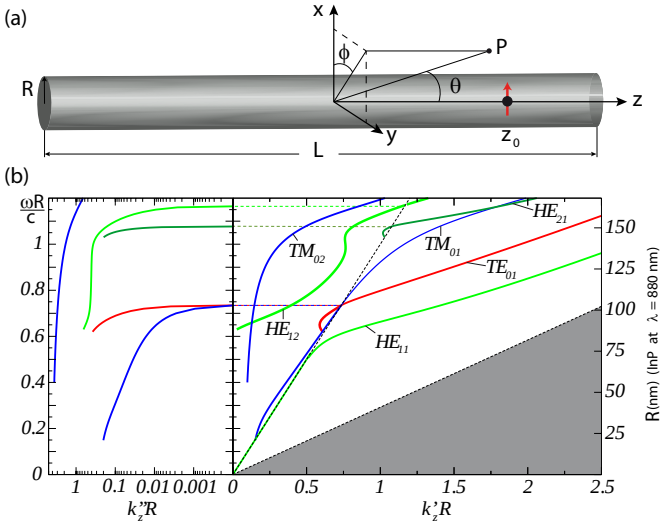

Fig. 1 (a) Scheme of the coordinate system and the relevant variables in the problem. (b) Right panel: Dispersion relation $\omega R/c$ vs $k_z'R$ from Eq. 1 for InP nanowires with varying radius R at $\lambda=880$ nm (refractive index $n_c=n_{\rm InP}=3.42$). Conversely, the dispersion relation applies to a proper spectral dependence for a fixed radius InP NW, as long as $n_{\rm InP}$ remains constant. Left panel: Imaginary part of leaky modes (correspondence indicated by horizontal dashed lines) expressed through $\omega R/c$ vs $k_z''R$.

those modes with $k_z<\omega/c$ leak out of the NW due to the non-negligible real part of the wavevector component in the plane perpendicular to the NW axis ($k=0$). Actually, such leaky modes posses a non-zero imaginary part of the parallel wavevector k_z even for non-absorbing NWs. This $k_z=0$ stems from the very *leaky* nature of the mode, accounting indeed for losses due to leakage of energy along propagation (k_z being inversely proportional to the decay length of the mode along the NW axis). Thus k_z corresponding to the first few leaky modes is also plotted (see left panel in Fig. 1(b)). On the other hand, note that leaky modes are continued outside the light cone into guided modes, since their symmetry is preserved (same notation in Fig. 1).

In the case of $m=0$ in Eq. 1, transverse magnetic (TM_{0l}) and electric (TE_{0l}) modes are decoupled, corresponding, respectively, to the zeroes of the two terms in the left-hand side of the Eq. 1. Their magnetic (respectively, electric) fields are contained in the plane perpendicular to the NW axis, the integer l denoting their radial symmetry. If $m=0$ in 1, modes are no longer decoupled, their transverse electromagnetic field exhibiting a more complex symmetry. Particularly relevant is the lowest ($m=1$) electromagnetic mode, referred to as HE_{11}, exhibiting no cutoff in the low energy limit $\omega=0$.

With the help of the leaky/guided mode dispersion relation in Fig. 1, we will now investigate the photoluminescence of an arbitrarily placed/oriented dipole emitter located inside a finite

View Article Online
DOI: 10.1039/C3NR03001F

semiconducting nanowire. It is expected that the corresponding mode governs the emission process in various manners. On the one hand, the emission may be enhanced/inhibited in accordance with dipole emitter orientation and position. Calculated radiated powers exhibit large enhancements when the emitter is located at a position and orientation yielding large EM local density of states (LDOS). Conversely, strong inhibition occurs for position/orientation yielding vanishing LDOS. On the other hand, the NW mode properties will also influence the far field distribution, giving rise to a wealth of patterns that strongly depends on the NW length and dipole position, some of which can be exploited for ad-hoc directional emission.

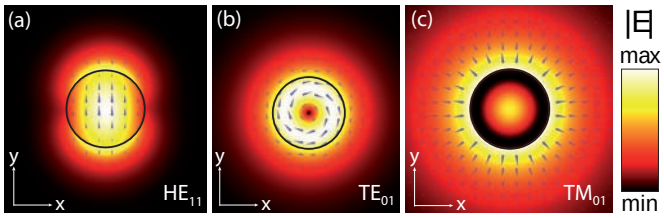

Fig. 2 Color maps of the electric field norm of the three guided modes supported by an infinite InP nanowire with radius $R = 126$ nm at $\lambda = 880$ nm (refractive index $n_{\mathrm{InP}} = 3.42$) , which corresponds to $\omega R/c = 0.9$ in Fig. 1. The arrows represent the direction of the in-plane components of the electric field, with size proportional to the norm. (a) HE_{11}, (b) TE_{01} and (c) TM_{01}.

3 Guided modes: Strong dependence on NW length and emitter position/orientation

First, various configurations are studied for which a guided mode plays a predominant role, manifesting a richer and more subtle phenomenology with regard to NW antenna emission, as compared to that of leaky modes[22]. To this end, we choose two cases from the dispersion relation in Fig. 1, at which guided modes are excited: $\omega R/c = 0.7$ and 0.9. This corresponds to InP NWs of radii $R = 98$ nm and 126 nm, respectively, at $\lambda = 880$ nm. First, we determine the symmetry of the three modes supported by the corresponding infinite InP nanowire of larger radius $R = 126$ nm in Fig. 2: HE_{11}, TE_{01}, and TM_{01}. Recall that the electromagnetic LDOS is related to the electric field pattern of the supported modes. The HE_{11} is the no cutoff mode discussed above with mixed EM character; the other two guided modes, TE_{01} and TM_{01}, are transverse electric ($E_z = 0$) and magnetic ($H_z = 0$), respectively. The thinner InP NW of radius $R = 98$ nm only supports the HE_{11} and TE_{01} guided modes, since the TM_{01} mode becomes leaky.

Next, we plot in Fig. 3 the total radiated power P for varying NW length L for classical point dipoles located at the NW center with either parallel or perpendicular orientations, numerically calculated by means of FEM simulations (COMSOL, as described in the Appendix). Recall that, the normalized total radiated power P/P_0 (where P and P_0 are the total powers emitted by the classical point dipole inside the NW and in a homogeneous InP medium, respectively), which yields the radiative decay rate enhancement γ_r/γ_{r0} is equivalent, for lossless media and 100% quantum efficiency (no non-radiative decay channels allowed), to the total decay rate enhancement $\gamma/\gamma_0 = \Gamma$, namely, to the properly defined Purcell factor Γ. It is evident from Fig. 3 that the NW plays also the role of a Bragg cavity, so that a standing (guided) wave is formed inside the NW that makes the LDOS oscillate along the NW length. Interestingly, different oscillations are observed depending on dipole orientation: a period of 355 nm (507 nm, respectively) is observed for a dipole perpendicular to the NW axis for $\omega R/c = 0.9$ ($\omega R/c = 0.7$, respectively) with enhancements up to ~ 4 (Figs. 3(a) and 3(b)), whereas that of the parallel dipole is much longer, 825 nm (888 nm, respectively), but slightly inhibited ($P/P_0 \lesssim 1$, Figs. 3(c) and 3(d)). This is a clear indication that different modes are being excited.

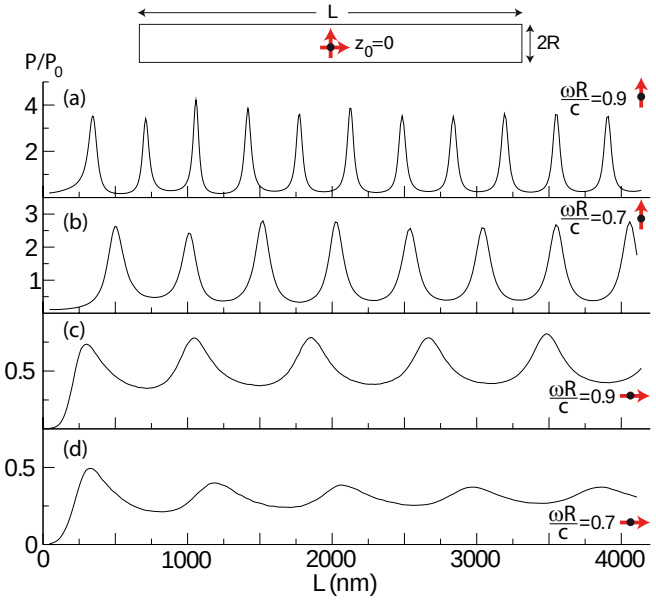

Fig. 3 Total radiated power P, normalized to that in a homogeneous InP medium P_0, as a function of NW length L for perpendicular, (a)-(b), and parallel, (c)-(d), dipoles placed at the NW center. Two configurations are considered with $\omega R/c = 0.9, 0.7$, corresponding to InP NWs with radii $R = 126, 98$ nm at $\lambda = 880$ nm.

Let us further explore this point in light of the dispersion relation (Fig. 1) and supporting mode symmetries (Fig. 2). Since the dipoles are located at the NW center, we expect no coupling at all to the TE_{01} guided mode, for its electric field amplitude is null there. The parallel dipole should couple to the TM_{01} mode (maximum electric field amplitude parallel to the

View Article Online
DOI: 10.1039/C3NR03001F

NW axis at the NW center), whereas the perpendicular dipole couples to the HE_{11} mode. This agrees perfectly with the dispersion relation, which yields the following wavelengths for the presumably excited guided modes: (i) $\lambda_z = 2\pi/k_z$ =825 nm and 888 nm for the TM_{01} mode at $\omega R/c = 0.9$ and 0.7, respectively; (ii) $\lambda_z = 2\pi/k_z$ =355 nm and 507 nm for the HE_{11}, respectively. Moreover, the TM_{01} mode is a leaky mode for the NW with $\omega R/c = 0.7$, as mentioned above, but with a large propagation length. This is also revealed by the attenuation of the total radiated power oscillations with increasing L.

To confirm such selective guided-mode coupling, we calculate the near-field associated with the perpendicular and parallel dipole emission for a finite InP NW $\omega R/c = 0.9$ in Fig. 4. Oscillations are found along the (NW) z-axis that exactly match the wavelengths of the HE_{11} and the TM_{01} modes, as mentioned above, but now revealed in the z-dependence for fixed NW length L (Figs. 4(a) and 4(b)). Correspondingly, the cross sections of the electric field norm in the plane perpendicular to the NW axis ((Figs. 4(c) and 4(d)) resemble very closely those of the HE_{11} and the TM_{01} modes for infinitely long NWs (Figs. 4(e) and 4(f)).

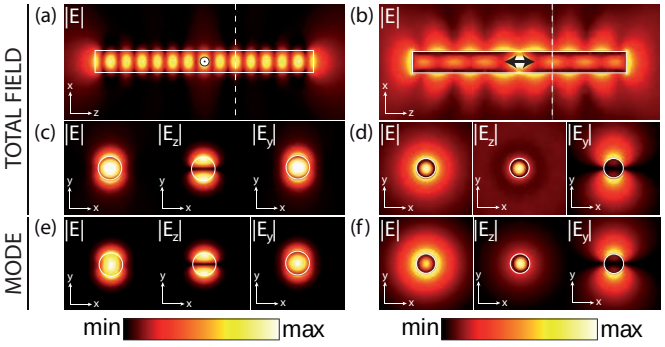

Fig. 4 Near-field snapshots of the electric field norm of the dipole emission at $\lambda = 880$ nm from an InP nanowire of width $R = 126$ nm ($\omega R/c = 0.9$) and length $L = 2.485\,\mu$m (so that $L = 7\lambda_z^{HE_{11}}$). Left panel: perpendicular; right panel: parallel. Cross sections are shown both along the NW axis, (a)-(b), and in the plane perpendicular to it (at the z position denoted by the white vertical dashed lines, (c)-(d)), in the later case including all electric field components separately. The guided mode EM field patterns for the HE_{11} mode,(e), and the TM_{01} mode, (f), supported by an infinite InP NW at the same radius are also included for comparison.

In order to give some physical insight into the emission process, we make use of simple expressions assuming that the emission is similar to that of a quasi-1D finite line current $I(z)$ (by modeling the semiconducting NW antenna as a 1D cavity with length L), as done for metallic nanorods in Ref.[34], extended hereby to account for all dipole orientations (and related mode symmetries). In our case, only displacement currents are assumed to be originating the far field emission. These currents can be polarized either along the NW axis $\mathbf{I} = I(z, z_0)\hat{\mathbf{z}}$ (TM_{01} mode excitation) or perpendicular to it $\mathbf{I} = I(z, z_0)\hat{\mathbf{y}}$ (HE_{11} mode excitation). This scenario accounts for the predominant component of the displacement currents of each mode. In both cases, $I(z, z_0)$ is given by:

$$I(z, z_0) = I_0 \frac{e^{\imath k_z z_0} \pm r e^{\imath k_z L} e^{-\imath k_z z_0}}{1 - r^2 e^{2\imath k_z L}} \times (r e^{\imath k_z L} e^{\imath k_z z} - e^{-\imath k_z z}), \quad \text{for } -L/2 \le z < z_0, \quad (2a)$$

$$I(z, z_0) = I_0 \frac{r e^{\imath k_z L} e^{\imath k_z z_0} \pm e^{-\imath k_z z_0}}{1 - r^2 e^{2\imath k_z L}} \times (e^{\imath k_z z} - r e^{\imath k_z L} e^{-\imath k_z z}), \quad \text{for } z_0 < z \le L/2, \quad (2b)$$

where the $\pm$ sign depends on the dipole character (electric or magnetic) and the specific mode being excited.

In determining the current intensities $I(z, z_0)$ along the NW length L, resulting from a dipole emitter located at z_0, the k_z wavevectors of the (presumably) excited guided modes are taken into account, along with proper reflection coefficients at the NW ends. For currents with polarization along the NW axis, the only component of the electric far field is:

$$E_\theta = \frac{\imath k_0 \eta_0}{4\pi} \sin\theta \int_{-L/2}^{L/2} I(z, z_0) e^{-\imath k_0 z \cos\theta} dz, \quad (3)$$

where η_0 stands for the vacuum impedance. The far-field thus obtained necessarily exhibits NW-axial symmetry (no az-

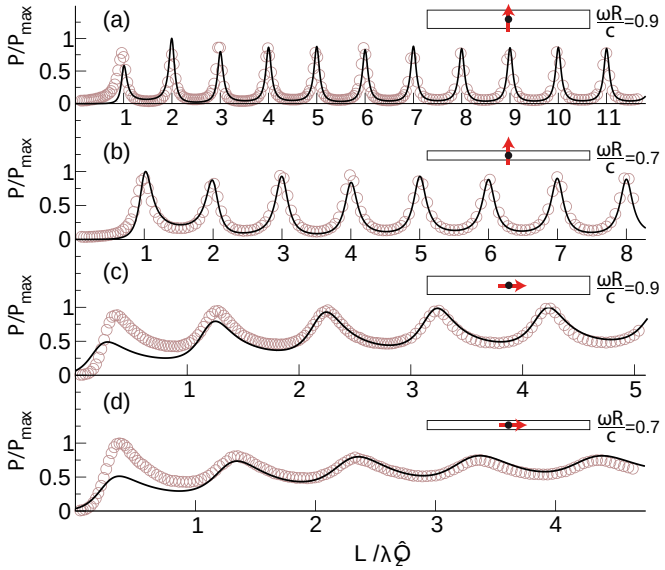

Fig. 5 Normalized total radiated power $P/P_{\max}$ (hollow symbols) as in Fig. 3, but rescaling the NW length L by the corresponding guided mode wavelength $\lambda_z = 2\pi/k_z'$: HE_{11} for the perpendicular dipoles, (a) and (b), and TM_{01} for parallel dipoles, (c) and (d). The fits to the quasi-1D current emission model are shown as solid curves.

View Article Online
DOI: 10.1039/C3NR03001F

imuthal dependence). Nevertheless, for dipoles perpendicular to the NW axis (thus exciting the HE_{11} mode), the far-field pattern does depend on both θ and ϕ as follows:

$$E_\theta = \frac{\imath k_0 \eta_0}{4\pi} \cos\theta \sin\phi \int_{-L/2}^{L/2} I(z, z_0) e^{-\imath k_0 z \cos\theta} dz \quad (4a)$$

$$E_\phi = \frac{\imath k_0 \eta_0}{4\pi} \cos\phi \int_{-L/2}^{L/2} I(z, z_0) e^{-\imath k_0 z \cos\theta} dz. \quad (4b)$$

The angular ditribution of the radiated power is simply given by:

$$S(\theta, \phi) \ = \frac{1}{2} c \epsilon_0 \ \mathbf{E}\ ^2, \quad (5)$$

from which the total radiated power is obtained by integration in the solid angle.

Good agreement is found, as shown in Fig. 5. The results are shown as a function of NW length rescaled by the the corresponding guided mode wavelength $\lambda_z = 2\pi/k_z$: HE_{11} for the perpendicular dipoles, Figs. 5(a) and 5(b), and TM_{01} for the parallel dipole, Figs. 5(c) and 5(d). Note that the maxima of the Purcell factor oscillations for perpendicular dipoles occur always at NW lengths that are integers of the HE_{11} mode wavelength, unlike the case of the parallel dipoles in terms of the TM_{01} mode wavelength, that are slightly shifted. In the former case, the effective reflection coefficient r at the NW end is real, whereas in the latter case a phase ought to be introduced (or, alternatively, an effective length different from L). Although r can be numerically computed[37], here we have obtained it as the only fitting parameter in Eq. (2). Interestingly, as pointed in Ref.[37], r grows as the HE_{11} mode becomes increasingly confined and does not depend on the length of the NW. It, moreover, approaches the reflection coefficient of a plane wave at dielectric/air interface at normal incidence ($r \sim 0.5$ at $\omega R/c = 0.7$, and $r \sim 0.55$ at $\omega R/c = 0.9$). The phase introduced upon reflection for the TM_{01} mode does not depend on the NW length but it does, also, on the confinement of the mode. In both cases, this agreement not only supports the use of such simple model for describing the emission pattern, but also confirm indirectly that the NW photoluminescence is to be governed by a given guided mode in a predictable manner.

We now explore the dependence of dipole emitter position for a fixed NW length. Bear in mind that such possibility is experimentally feasible in at least two manners: by selectively exciting/pumping a narrow, subwavelength area of the NW through cathodoluminescence[38,39]; or by limiting the size of the emitting material. The latter can be achieved by embedding a narrow heterostructure[40,41] or a quantum-dot[3,42] in an otherwise non-emitting NW. Results for a perpendicular dipole in an InP NW at $\omega R/c = 0.7$ are shown in Fig. 6. A similar oscillatory behavior is retrieved throughout the NW

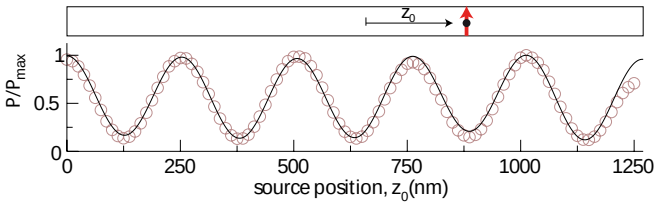

Fig. 6 Normalized total radiated power $P/P_{\max}$ (hollow symbols) as a function of dipole position z at the NW axis for a perpendicular dipole in an InP NW with fixed length $L = 2.54\,\mu$m and radius $R = 98$ nm at $\lambda = 880$ nm ($\omega R/c = 0.7$), together with the prediction of the 1D current emission model (solid curve).

length, with only a slight perturbation near the NW end. Such behavior can be also described by means of the above model, as corroborated by the good agreement with the fitting curves in Fig. 6. It should be remarked that the enhancement factor is strongly dependent on dipole position due to the coupling to guided modes, unlike for leaky mode excitation (discussed below).

Finally, we investigate the behavior of the angular distribution of emitted light, crucial to tailor photoluminescence directionality. As expected, the far-field pattern also reveals such cavity effect through various lobes, as observed in Fig. 7 for various configurations. The number of such lobes is related to the NW length and guided mode wavevector. (Incidentally, note that polar lobes are only obtained for perpendicular dipoles in the case that the HE_{11} mode is excited; the symmetry of the TM_{01} guided mode, with the electric field pointing perpendicular to the NW end facet precludes such polar emission.) In this regard, the NW length and radius can be chosen so that a particular guided mode is excited with enhanced emission, tuning in turn the number and position of maxima of the angular radiated power. Therefore, strong, highly directional lobes can be obtained, the semiconducting nanowire thus playing the role of a nanoantenna[22]. For instance: for perpendicular dipole orientation, Figs. 7(a)-(d), polar lobes concentrating most of the power are present in (b) or (c), while polar radiation is almost entirely suppressed in (a) or (d); for parallel dipole emission, large conical lobes with axial symmetry (with tunable width and polar angle as in Figs. 7(e)-(f)) can be obtained; etc. Again note that the emission patterns are in excellent agreement with the predictions from Eqs. (3) and (4). With regard to the dependence on dipole position, note that, if $r = 1$ in Eqs. (2), the angular pattern is preserved up to a constant (enhancement/inhibition) factor. Otherwise, the number and position of lobes are also preserved, but their relative intensity might vary.

Thus far, dipole emitters have always been located at the NW center. By displacing the dipole emitter from the NW center (see Fig. 8), symmetry considerations are again nec-

View Article Online
DOI: 10.1039/C3NR03001F

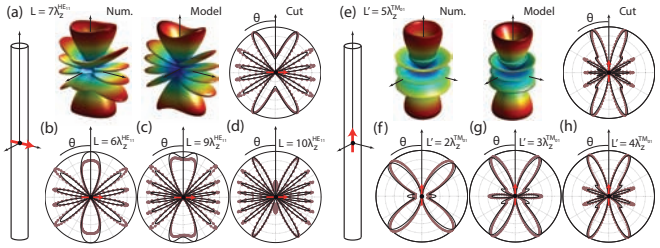

Fig. 7 Far-field angular radiated power from finite InP NWs with perpendicular, (a)-(d), and parallel, (e)-(h), dipoles located at the NW center. Several NW lengths are considered, all with $\omega R/c = 0.9$, corresponding to NWs with radii $R = 126$ nm at $\lambda = 880$ nm. In (a) and (e) a full 3D plot is included to illustrate the azimuthal dependence for the perpendicular dipole, and the axial symmetry for the parallel one, while in the remaining, (b)-(d) and (f)-(h), only polar-plane projections are shown. Both full numerical simulations (curves with symbols) and 1D current emission model results (solid curve) are included.

essary in order to explain guided-mode outcoupling. If the

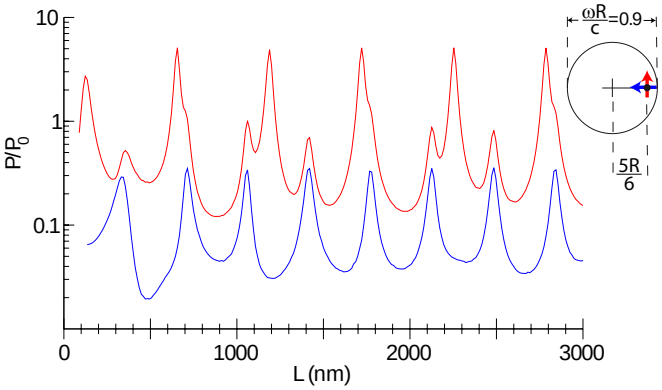

Fig. 8 Total radiated power P/P_0 as a function of NW length L for (axial and radial) perpendicular dipoles placed off the NW center with $\omega R/c = 0.9$, corresponding to an InP NW with radius $R = 126$ nm at $\lambda = 880$ nm. The dipoles are placed at a distance $5R/6$ from the NW center.

off-center dipole is axially oriented, a doubly oscillating pattern is observed with two periods: a strong component with period ~ 530 nm and a weak component with period ~ 350 nm. The strong component clearly reveals coupling into the TE_{01} guided mode, of wavelength $\lambda_z = 2\pi/k_z = 531$ nm at $\omega R/c = 0.9$, with enhancement factors $\Gamma \sim 5$, due to the fact that such mode exhibits in-plane, axially rotating electric field amplitude that is maximum away from the NW center (see Fig. 2). In addition, weak coupling into the HE_{11} mode ($\lambda_z = 355$ nm) is observed, as expected. This argument is confirmed by the results of the off-center, radially oriented dipole, whose radial symmetry precludes TE_{01} mode excitation, yielding only weak coupling into the HE_{11} mode. Although cupling to TM_{01} mode is not forbidden by symmetry (see Fig. 2), the in-plane electric field components are very weak compared to the in-plane components of the mentioned HE_{11} mode (recall that for TM_{01} mode most of the electric field is parallel to the NW axis. The case of the parallel, off-center dipole (not shown here) trivially yields the expected coupling into the TM_{01} mode, though weaker than that of the centered dipole (Fig. 3), and into the HE_{11} mode.

In summary, (electric dipole) emission enhancement and directionality can be tailored at the required vacuum photoluminescence wavelength by tuning the NW radius and length; the so called semiconductor NW antenna-like behavior, experimentally demonstrated previously through leaky mode coupling[22], is far richer upon exploiting guided-mode coupling and can be easily described in terms of the emission of a quasi-1D finite line current. Even if the photoluminescence is randomly emitting, note that the NW parameters can be optimized so that coupling into a particular mode is enhanced. Moreover, if selective emission from a particular NW position can be achieved, the emission can be tailored even for a fixed NW length. On the other hand, if photoluminescence were originated uniformly throughout the entire NW, the resulting emission could be obtained by incoherently averaging the dipole emission over space, polarization, and over all excited modes. For instance, by spatially averaging over the position-dependent enhancement factor of Fig. 6, an overall enhancement of P/P_0 1.5 is found (with respect to homogeneous InP, being larger $1.5n_{\mathrm{InP}}$ if normalized to emission in vacuum).

4 Leaky modes: Weak dependence on NW length and emitter position

Next, we consider the case in which only a leaky mode is excited. Moreover, we assume that the nanowire is longer than the leakage length of the mode, which can be obtained from the inverse of k_z (see Fig. 1, left graph). Note that, if the nanowire length is shorter than the leakage length, the phenomenology is similar to that involving the excitation of a guided mode, as discussed above.

Let us focus in Fig. 9 on an InP nanowire of width $R = 50$ nm ($\lambda = 880$ nm, $\omega R/c = 0.37$); apart from the no-cutoff HE_{11} mode, very weakly guided at such $\omega R/c$, the only mode supported is the leaky TM_{01} mode (see Fig. 1). Actually, the TM_{01} mode symmetry (see Fig. 2 above for the corresponding TM_{01} guided mode, bearing in mind that the symmetry is preserved) imposes that the emission from a dipole oriented parallel to the NW axis is selectively enhanced with respect to that of the perpendicular orientation (not shown), as pointed out in Ref.[22]. Due to the leaky nature of the mode, the dipole posi-

View Article Online
DOI: 10.1039/C3NR03001F

tion along the NW does not play a significant role, enhancement/inhibition being nearly uniform (P/P_0 0.6), as shown in Fig. 9(a). Indeed, the experimental results reported in Ref.[22] confirm this point, through the following argument: since NW excitation was nearly uniform, uniform emission was assumed in turn. The calculations were done by placing a single dipole (3 orientations considered) at the NW center, reproducing the experimental results very accurately, both quantitative (enhancement/inhibition) and qualitatively (directionality), thanks to the fact that the leaky-mode-induced photoluminescence is nearly independent of the dipole position. (Incidentally, this can be further verified by spatial averaging the emission over dipole position and orientation throughout the NW, confirming that the resulting averaged emission is nearly identical to that of single, randomly oriented, centered-dipole emission.)

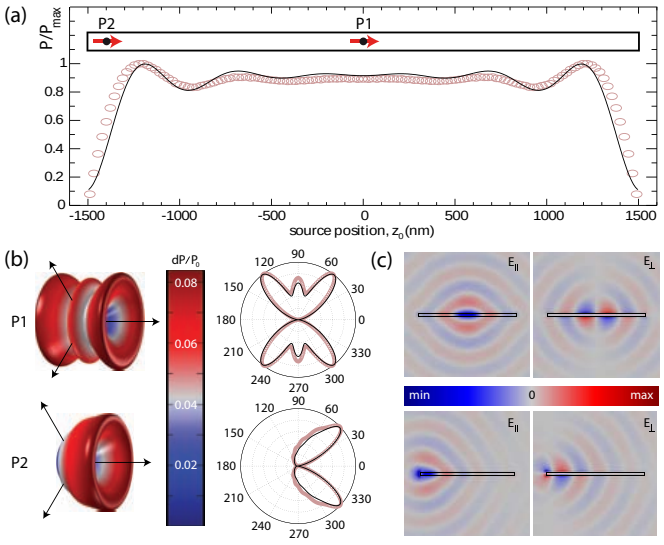

Fig. 9 (a) Normalized radiated power (hollow symbols) as a function of (parallel) dipole position z at the NW axis for a finite ($L = 3\,\mu$m) InP nanowire with $R = 50$ nm at $\lambda = 880$ nm ($\omega R/c = 0.37$, at which only the TM_{01} leaky mode is excited), along with the 1D current emission model prediction (solid curve). The inset represents the positions inside the NW for which the emission properties will be studied. (b) Total and projected far-field intensities of the light emitted by two dipoles, located at either the NW center (P1) or close to the NW edge (P2, at a distance $d = 100$ nm), together with the 1D current emission model (projections only). (c) The corresponding emission snapshots in the near-field map.

Here we plot in Fig. 9 such far-field pattern at $\lambda = 880$ nm for a free standing, finite InP NW of width $R = 50$ nm and length $L = 3\,\mu$m. The doughnut shape associated to dipole emission is deformed as due to the NW antenna effect induced by the TM_{01} leaky mode excitation, exhibiting three axial lobes for the parallel dipole (the configuration obviously imposes axial symmetry); unlike in the case of the vertical NW on a planar substrate[22], where the equatorial ring was outside the angular range of the objective numerical aperture of the Fourier microscope (so that a single ring appeared in the Fourier image). The perpendicular dipole does not couple to the TM_{01} leaky mode, so that its dipolar emission is only slightly inhibited and deformed.

Nonetheless, if the dipole emitter is very close to the NW end (closer than its propagation length), the far-field distribution is deformed in a different manner (see Fig. 9). (Note that this was not observed in Ref.[22] for the overall contribution from both NW ends is negligible.) A single axial lobe is obtained (sort of an upside down cup), directed towards the NW (north) pole opposite to the dipole emitter location, stemming from the bouncing of the excited TM_{01} leaky mode off the NW end (south pole).

We have also exploited the quasi-1D displacement current model through Eqs. (2-4), assuming in this case that the k_z wavevector is complex, as given by the excited TM_{01} leaky mode from Eq. 1, to reproduce the total power and the far field patterns (Fig. 9), with very good agreement.

Therefore, leaky mode excitation modifies qualitative and quantitatively photoluminescence, inducing a NW antenna-like effect, confirming previous experimental results[22]. Indeed, emission can be tailored to a certain degree through the dipole position/orientation (compared to mode symmetry). However, the emission is weakly modified upon varying the dipole position along the NW length, unless the dipole is located very close to the NW edge.

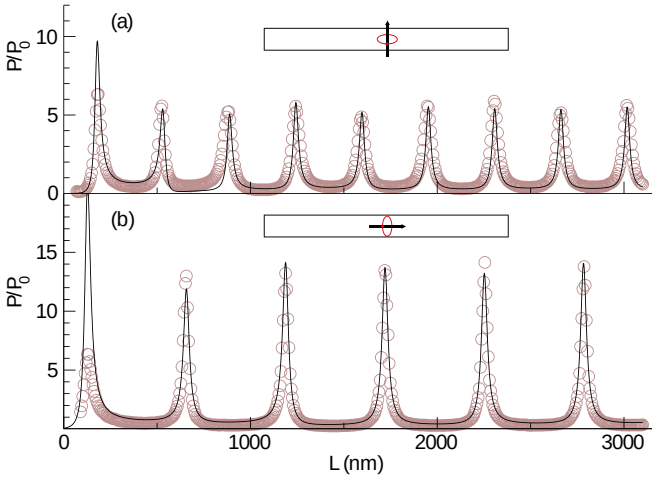

Fig. 10 Radiated power enhancement P/P_0 as a function of NW length L for perpendicular, (a), and parallel, (b), magnetic dipoles placed at the NW center with $\omega R/c = 0.9$, corresponding to an InP NW with radius $R = 126$ nm at $\lambda = 880$ nm. The results of the 1D current emission model are also shown.

View Article Online
DOI: 10.1039/C3NR03001F

5 Magnetic dipole emitter

Recall that magnetic dipole transitions indeed mediate spontaneous emission from lantanides[35], which hold promise of applications in a range of technologies from lighting and displays to lasers and fiber amplifiers. Let us analyze the NW length dependence of the radiative power modulation for perpendicular and parallel (centered) magnetic dipoles, as shown in Figs. 10(a) and 10(b), respectively. Emission should now be governed by the magnetic LDOS[43], taking into account that the supported modes exhibit the magnetic field patterns shown in Fig.11. This is clearly observed in the case of the parallel dipole in Fig. 10(b): $P(L)$ shows an oscillating behavior (period ∼530 nm) as a result of the coupling into the TE_{01} mode, which is the only one that has a large non-zero magnetic LDOS along the NW axis at the center (see Fig. 11(b)). Conversely, the perpendicular magnetic dipole coupling into the TE_{01} mode is forbidden by magnetic LDOS symmetry, its emission being thus governed by the coupling into the HE_{11} mode. Magnetic dipole emission can also be fitted to the quasi-1D current model finding good agreement, as shown in Fig. 10. Remarkably, maximum radiative enhancement factors of the order of $\sim 5-20$ are achieved, which might be exploited to enhance (and also to steer) the (typically weaker) magnetic dipole emission[35].

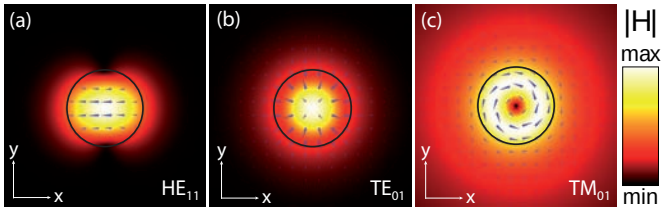

Fig. 11 Contour maps of the magnetic field norm of the three guided modes supported by an infinite InP nanowire with radius $R = 126$ nm at $\lambda = 880$ nm (refractive index $n_{\mathrm{InP}} = 3.42$) , which corresponds to $\omega R/c = 0.9$ in Fig. 1. The arrows represent the direction of the in-plane components of the magnetic field, with size proportional to the norm. (a) HE_{11}, (b) TE_{01} and (c) TM_{01}.

6 Concluding remarks

In this work, we have investigated theoretically and numerically the photoluminescence performance of finite semiconducting NWs. Incidentally,NW material quality should be considered in different manners. Typically, NWs form in single crystals; even if defects/stacking faults are present, they are subwavelength at optical wavelengths and thus nearly irrelevant. If any, a slight modification of the real and imaginary components of the refractive index could be observed due to defects in the real material that might modify the crystal electronic band structure, mostly by introducing new emission peaks that become less relevant at room temperature[19,44,45], resulting only in a slight modification of the mode dispersion relation. Also, if the NW surface is rough, the mode scattering out of the NW (roughness-induced leakage) might deteriorate performance. However, considering present state-of-the-art material quality, this is not an issue for the emission properties. For instance, perfect single-crystalline (zincblende) InP was assumed in the numerical calculations in Ref.[22], whereas wurtzite (or a mixture) was the NW material in the actual experiment: the agreement was notable.

In summary, on the basis of the leaky/guided mode dispersion relation for infinite NWs, the light emission from finite nanowires is theoretically and numerically studied for specific configurations that optimize coupling into leaky or guided modes. In particular, especial emphasis is put on the conditions that yield larger enhancement factors and desired directionality, so called nanowire antenna effect[22]. A wealth of phenomenology is predicted and explored when guided modes are excited, with strongly oscillating dependence on NW length, (electric and magnetic) dipole position and orientation, in turn governed by the properties of the corresponding guided mode. Physical insight into such behavior is given by through a simple, quasi-1D cavity emission model for various mode symmetries and dipole orientations. In contrast, leaky mode excitation is shown to be largely independent of the dipolar emitter within the nanowire, although enhanced and directional emission can also be achieved. This theoretical work, supported by rigorous numerical simulations, sheds light onto the optical properties of semiconductor nanowires in general, providing a consistent framework to predict/tailor photoluminescence (enhancement and directionality), with crucial implications in a variety of Nanowire photonics applications: light-emitting devices, single-photon sources, nanolasers, etc.

Acknowledgments

We are grateful to Luis Froufe-Pérez for his careful reading of the manuscript. The work of Ramón Paniagua-Dom´nguez and José A. Sánchez-Gil has been supported in part by the Spanish "Ministerio de Econom´a y Competitividad" (projects Consolider-Ingenio EMET CSD2008-000666 and NANOPLAS+ FIS2012-31070) and the "Comunidad de Madrid" (MICROSERES network S-2009/TIC1476). Ramón Paniagua-Dom´nguez acknowledges support from CSIC and the European Social Fund through a JAE-Pre grant. This work is also part of the research program of the "Stichting voor Fundamenteel Onderzoek der Materie (FOM)", which is financially supported by the "Nederlandse organisatie voor Wetenschappelijk Onderzoek (NWO)" and is part of an industrial partnership program between Philips and FOM.

View Article Online
DOI: 10.1039/C3NR03001F

Appendix

Finite-element-method-based numerical simulations were performed using commercial software COMSOL Multyphysics v4.3. For NWs of length L larger than one micron, the simulated space consisted on a circular cylinder of length L and diameter $2R$, representing the nanowire, and two concentric spheres of radii $0.7L$ and $1.1L$, respectively, with their centers coinciding with that of the cylinder. In the outter sphere an additional spherical layer of thickness $0.2L$ was defined. Aside from the cylinder, this geometry divides the simulation space into three concentric spherical subdomains, as shown in Fig. 12(a). They were all set to be air ($n_{Air} = 1$). The outter spherical layer was define as a perfectly matched layer (PML) to absorb all the outgoing radiation. For the cylinder representing the NW, material constants for InP were taken from Palik s book[36].

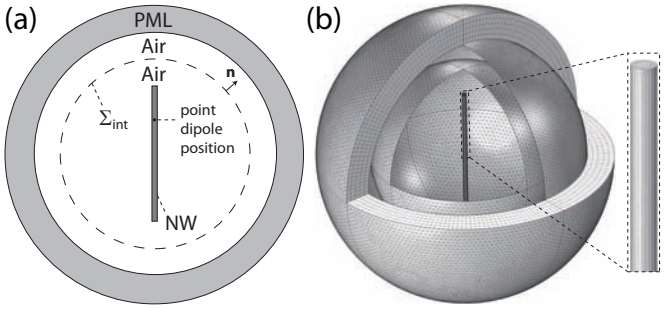

Fig. 12 (a) Cross section of the domains used in COMSOL numerical simulations. (b) Illustration of the domain meshing.

The meshing was done with the program built-in algorithm, which creates a tetrahedral mesh. The mesh maximum element size (MES), which limits the maximum size of the edges of the tetrahedrons, was set to be 20 nm in the domain representing the wire, and 80 nm for all the elements in the air subdomains. The maximum element growth rate was set to 1.35 in all domains (see Fig. 12(b)). Direct PARDISO solver was used to solve the problem. Simulations were highly memory demanding (typically more than 150 GB) and time consuming, depending on the nanowire particular length.

In the inner spherical boundary, Σ_{int}, additional post-proccesing calculations are performed, as the computation of the total radiated power, P, defined by:

$$P = \int_{\Sigma_{int}} \mathbf{S} \cdot \mathbf{n} dS, \qquad (6)$$

$\mathbf{n}$ being the outward normal unit-vector to the surface.

References

1 R. Yan, D. Gargas and P. Yang, *Nature Photonics*, 2009, **3**, 569–576.
2 J. Claudon, N. Gregersen, P. Lalanne and J.-M. Gerard, *ChemPhysChem*, 2013, doi: 10.1002/cphc.201300033.
3 J. Claudon, J. Bleuse, N. S. Malik, M. Bazin, N. Gregersen, C. Sauvan, P. Lalanne and J.-M. Gerard, *Nature Photonics*, 2010, **4**, 174–177.
4 T. M. Babinec, B. J. M. Hausmann, M. Khan, Y. Zhang, J. R. Maze, P. R. Hemmer and M. Loncar, *Nature Nanotechnology*, 2010, **5**, 195–9.
5 M. Heiss, Y. Fontana, A. Gustafsson, G. Wüst, C. Magen, D. D. O Regan, J. W. Luo, B. Ketterer, S. Conesa-Boj, A. V. Kuhlmann, J. Houel, E. Russo-Averchi, J. R. Morante, M. Cantoni, N. Marzari, J. Arbiol, A. Zunger, R. J. Warburton and A. Fontcuberta I Morral, *Nature Materials*, 2013, **12**, 439–444.
6 M. E. Reimer, G. Bulgarini, N. Akopian, M. Hocevar, M. B. Bavinck, M. A. Verheijen, E. P. A. M. Bakkers, L. P. Kouwenhoven and V. Zwiller, *Nature Communications*, 2012, **3**, 737.
7 M. H. Huang, S. Mao, H. Feick, H. Yan, Y. Wu, H. Kind, E. Weber, R. Russo and P. Yang, *Science (New York, N.Y.)*, 2001, **292**, 1897–9.
8 L. K. van Vugt, S. Ruhle and D. Vanmaekelbergh, *Nano Lett.*, 2006, **6**, 2707–2711.
9 D. Vanmaekelbergh and L. K. van Vugt, *Nanoscale*, 2011, **3**, 2783–2800.
10 J. Wang, M. S. Gudiksen, X. Duan, Y. Cui and C. M. Lieber, *Science (New York, N.Y.)*, 2001, **293**, 1455–7.
11 O. L. Muskens, J. Gómez Rivas, R. E. Algra, E. P. A. M. Bakkers and A. Lagendijk, *Nano Letters*, 2008, **8**, 2638–2642.
12 M. D. Kelzenberg, S. W. Boettcher, J. A. Petykiewicz, D. B. Turner-evans, M. C. Putnam, E. L. Warren, J. M. Spurgeon, R. M. Briggs, N. S. Lewis and H. A. Atwater, *Nature Materials*, 2010, **9**, 239–244.
13 L. Cao, P. Fan, A. P. Vasudev, J. S. White, Z. Yu, W. Cai, J. A. Schuller, S. Fan and M. L. Brongersma, *Nano Letters*, 2010, **10**, 439–45.
14 G. Bronstrup, N. Jahr, C. Leiterer, A. Csaki, W. Fritzsche and S. Christiansen, *ACS Nano*, 2010, **4**, 7113–7122.
15 J. Wallentin, N. Anttu, D. Asoli, M. Huffman, I. Aberg, M. H. Magnusson, G. Siefer, P. Fuss-Kailuweit, F. Dimroth, B. Witzigmann, H. Q. Xu, L. Samuelson, K. Deppert and M. T. Borgström, *Science (New York, N.Y.)*, 2013, **339**, 1057–1060.
16 P. Krogstrup, H. Q. Jörgensen, M. Heiss, O. Demichel, J. V. Holm, M. Aagesen, J. Nygard, and A. Fontcuberta i Morral, *Nature Photonics*, 2013, **7**, 306–310.
17 S. L. Diedenhofen, G. Vecchi, R. E. Algra, A. Hartsuiker, O. L. Muskens, G. Immink, E. P. A. M. Bakkers, W. L. Vos and J. Gómez Rivas, *Advanced Materials*, 2009, **21**, 973–978.
18 R. Paniagua-Dom´nguez, D. R. Abujetas and J. A. Sánchez-Gil, *Scientific Reports*, 2013, **3**, 1–7.
19 T. Ba Hoang, A. F. Moses, L. Ahtapodov, H. Zhou, D. L. Dheeraj, A. T. J. van Helvoort, B.-O. Fimland and H. Weman, *Nano Letters*, 2010, **10**, 2927–33.
20 S. L. Diedenhofen, O. T. A. Janssen, M. Hocevar, A. Pierret, E. P. A. M. Bakkers, H. P. Urbach and J. G. Rivas, *ACS Nano*, 2011, 5830–5837.
21 M. Munsch, J. Claudon, J. Bleuse, N. Malik, E. Dupuy, J.-M. Gérard, Y. Chen, N. Gregersen and J. Mørk, *Physical Review Letters*, 2012, **108**, 1–5.
22 G. Grzela, R. Paniagua-Dom´nguez, T. Barten, Y. Fontana, J. A. Sánchez-Gil and J. Gómez Rivas, *Nano Letters*, 2012, **12**, 5481–5486.
23 C. Wilhelm, A. Larrue, X. Dai, D. Migas and C. Soci, *Nanoscale*, 2012, **4**, 1446–1454.
24 J. A. Stratton, *Electromagnetic Theory*, McGraw-Hill Book Company, New York, 1941.
25 J. Arnbak, *Electronics Letters*, 1969, **5**, 41–42.
26 R. Sammut and A. W. Snyder, *Applied Optics*, 1976, **15**, 477–82.
27 K. Seo, M. Wober, P. Steinvurzel, E. Schonbrun, Y. Dan, T. Ellenbogen and K. B. Crozier, *Nano Letters*, 2011, **11**, 1851–6.
28 A. V. Maslov and C. Z. Ning, *Optics Letters*, 2004, **29**, 572–4.
29 A. V. Maslov, M. I. Bakunov and C. Z. Ning, *Journal of Applied Physics*,

View Article Online
DOI: 10.1039/C3NR03001F

2006, **99**, 024314.

30 I. Friedler, C. Sauvan, J. P. Hugonin, P. Lalanne, J. Claudon and J. M. Gérard, *Optics Express*, 2009, **17**, 2095–110.

31 O. L. Muskens, V. Giannini, J. A. Sánchez-Gil and J. Gómez Rivas, *Nano Letters*, 2007, **7**, 2871–2875.

32 V. Giannini and J. A. Sánchez-Gil, *Opt. Lett.*, 2008, **33**, 899–901.

33 V. Giannini, A. I. Fernández-Dom´nguez, S. C. Heck and S. A. Maier, *Chemical Reviews*, 2011, **111**, 3888–3912.

34 T. H. Taminiau, F. D. Stefani and N. F. V. Hulst, *Nano Letters*, 2011, **11**, 1020–1024.

35 S. Karaveli and R. Zia, *Physical Review Letters*, 2011, **106**, 193004.

36 E. D. Palik, *Handbook of Optical Constants of Solids*, Academic Press, 1998, vol. 3, p. 900.

37 A. V. Maslov and C. Z. Ning, *Applied Physics Letters*, 2003, **83**, 1237.

38 R. Sapienza, T. Coenen, J. Renger, M. Kuttge, N. F. van Hulst, and A. Polman, *Nature Materials*, 2012, **11**, 781–787.

39 T. Coenen, J. van de Groep, and A. Polman, *ACSNano*, 2013, **7**, 1689–1698.

40 A. Pierret, M. Hocevar, S. L. Diedenhofen,R. E. Algra, E. Vlieg, E. C. Timmering, M. A. Verschuuren, G. W. G. Immink, M. A. Verheijen, and E. P. A. M. Bakkers, *Nanotechnology*, 2010, **21**, 065305.

41 Y. Fontana, G. Grzela, E. P. A. M. Bakkers, and J. Gómez Rivas, *Physical Review B*, 2012, **86**, 245303.

42 M. T. Borgström, V. Zwiller, E. Müller, and A. Imamoglu, *Nano Letters*, 2005, **5**, 1439–1443.

43 K. Joulain, R. Carminati, J.-P. Mulet and J.-J. Greffet, *Physical Review B*, 2003, **68**, 245405.

44 A. Mishra, L. V. Titova, T. B. Hoang, H. E. Jackson, and L. M. Smith, J. M. Yarrison-Rice, Y. Kim, H. J. Joyce, Q. Gao, H. H. Tan, and C. Jagadish, *Applied Physics Letters*, 2007, **91**, 263104.

45 T. T. T. Vu, T. Zehender, M. A. Verheijen, S. R. Plissard, G. W. G. Immink, J. E. M. Haverkort and E. P. A. M. Bakkers, *Nanotechnology*, 2013, **24**, 115705.

View Article Online
DOI: 10.1039/C3NR03001F

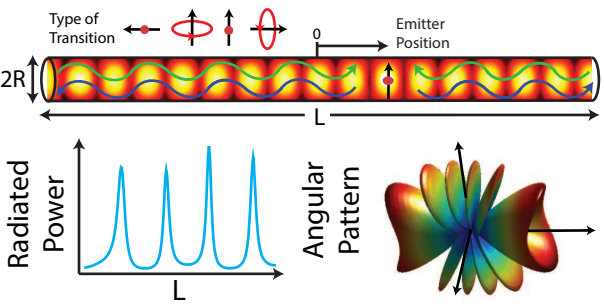

View Article Online
DOI: 10.1039/C3NR03001F

Table of content sentence:

Light emission from semiconductor nanowires is theoretically studied and related to the guided/leaky modes supported, yielding rules for optimization